Support Information

Photoformation of persistent free radicals on montmorillonite-humic acids complex simulated as particulate organic matter in aqueous solution.

Xintong Li [†], Chen Shen [†], Hongxia Zhao *[, †], Jingqiu Jiang [†], Zixin Ban, Zhenyu Chen, Baocheng Qu *[, ‡, §]

[†] Key Laboratory of Industrial Ecology and Environmental Engineering (Ministry of Education), School of Environmental Science and Technology, Dalian University of Technology, Linggong Road 2, Dalian 116024, China

[‡] Dalian Ocean University, Dalian 116023, China

[§]Key Laboratory of Environment Controlled Aquaculture, Ministry of Education, Dalian 116023, China

Text S1

The IR spectra of Mnt-HA-Cu^{2+} and Mnt-HA-2,4-DCP before and after irradiation were provided in Fig. S4. The characteristic peaks of -O-H occurred at ~3440 cm^{-1} and the characteristic absorptions of C=C bonds of aromatic rings or C=O groups appeared at ~1637 cm^{-1} in the IR spectra both before and after irradiation[1]. For Mnt-HA-Cu^{2+} complex, the relative absorption intensity of these groups decreased slightly after irradiation for 4 days. While for Mnt-HA-2,4-DCP complex, the intensity increased. This trend was consistent with our results that Cu^{2+} played a negative role and 2,4-DCP played a positive role on the photoformation of PFRs. A relatively weak signal at ~2970 cm^{-1} was observed for Mnt-HA-2,4-DCP before irradiation, which could be attributed to -CH_2- bonds of aliphatic structure[2, 3]. This suggested that the 2,4-DCP absorbed in the system could react with Mnt-HA and result in the decrease of the EPR signals. After irradiation for 4 days, the -CH_2- signal disappeared which revealed that the group might be involved in the photoformation of PFRs. The TG analyses of Mnt-HA complex were shown in Fig. S5. By comparing the TG curves of samples before and after irradiation, their trends in weight loss were similar and the rapid weight loss phase was not obvious, which was consistent with the previous research.[4] Only a weight loss beginning at around 50 ℃ and completing by ~200 ℃ with a relatively fast slope was observed and could be attributed to the loss of crystal water and coordinated water in the complex[5, 6]. It can be seen the weight loss is at around 19.2%, 20.5%, 18.5% and 22.1% for Mnt-HA-Cu^{2+} and Mnt-HA-2,4-DCP before and after irradiation respectively. The thermal stability of Mnt-HA complex before irradiation was slightly better than those after irradiation, which might prove the irradiation made samples more active.

Table S1 Parallel experiment data (n = 3) of Mnt-HA complex with transition metal ions (Cu^{2+}, Fe^{3+}, Zn^{2+}, and Mn^{2+}) under different irradiation time.

Irradiation time	2 d		4 d		6 d		8 d	
	Intensity (a.u.)	g-factor	Intensity (a.u.)	g-factor	Intensity (a.u.)	g-factor	Intensity (a.u.)	g-factor
Cu^{2+}	105022.3	2.00351	99194.8	2.0036	96207.9	2.00367	67478.1	2.00355
	104948.3	2.00351	97160.3	2.0036	92906.7	2.00367	63616.2	2.00355
	103463	2.0035	93657.3	2.00359	94645.5	2.00368	63124.5	2.00354
Fe^{3+}	105376.6	2.00358	135836.7	2.00362	133579.3	2.00365	127268	2.00365
	108719.1	2.00358	129881.6	2.00362	135366.6	2.00365	125060.5	2.00367
	104348.8	2.00358	126297.4	2.00361	132928.4	2.00366	123060	2.00366
Zn^{2+}	112946.9	2.00362	126938.7	2.00361	116184.6	2.0036	109980.2	2.00364
	110799.7	2.00362	124175.8	2.00361	115323.7	2.00361	107069.8	2.00364
	108914.3	2.00361	124809.5	2.00361	113956.1	2.0036	106803.6	2.00364
Mn^{2+}	63712.2	2.00354	54408.5	2.00355	61947.2	2.00364	74192	2.00366
	62318.5	2.00353	53818.4	2.00355	61794	2.00363	71295.4	2.00365
	62156.9	2.00353	53525.2	2.00355	61777.1	2.00363	71932.3	2.00365

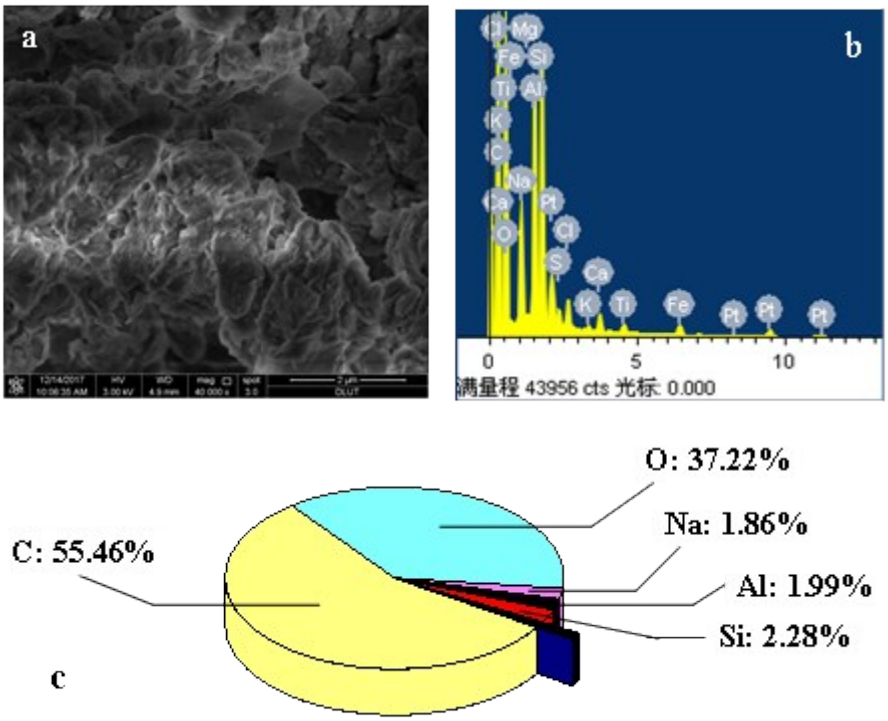

Fig. S1 Scanning electron microscope image (a) and elemental analysis image (b) of HA and the percentage of different elements in HA (c)

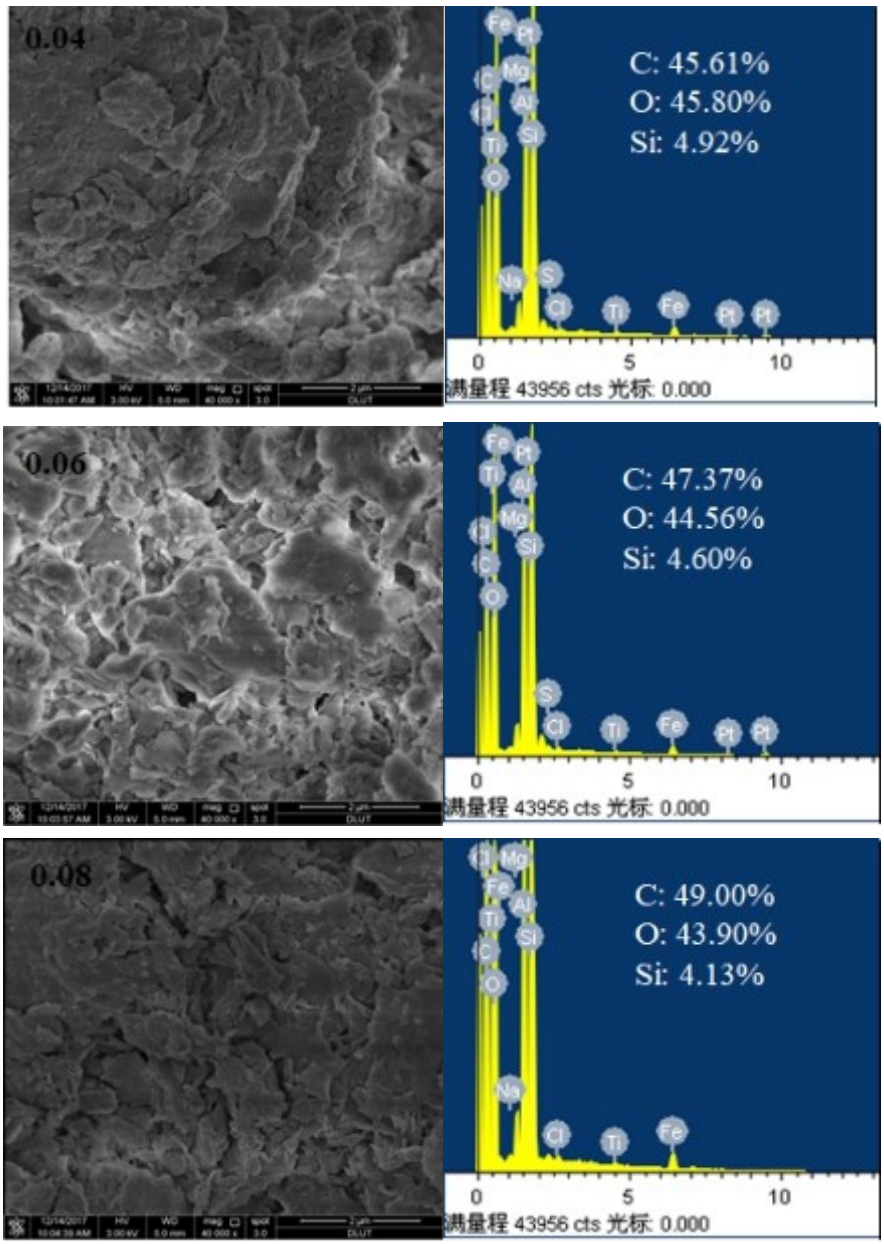

Fig. S2 Scanning electron microscope image and elemental analysis image of 0.04 Mnt-HA, 0.06 Mnt-HA and 0.08 Mnt-HA

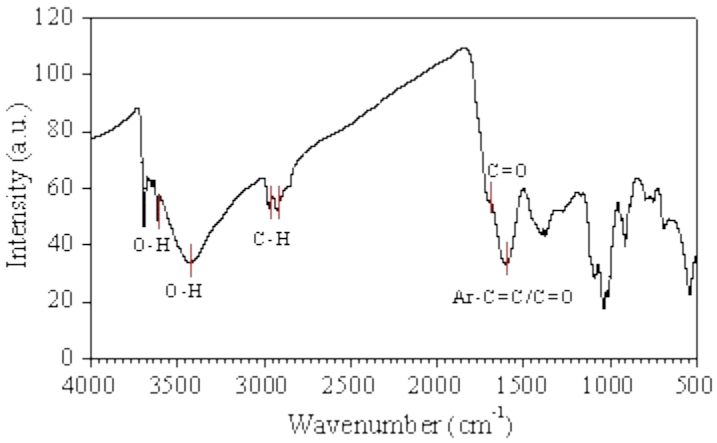

Fig. S3 Infrared spectrum of HA

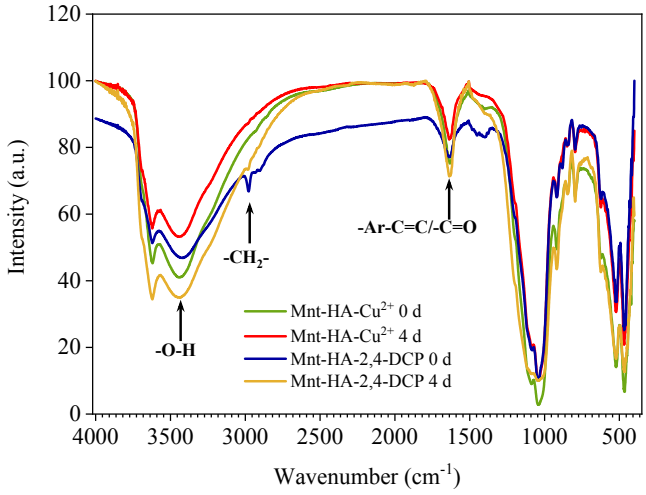

Fig. S4 Infrared spectrum of Mnt-HA-0.1 mM Cu^{2+} and Mnt-HA-2 mM 2,4-DCP samples before and after irradiation for 4 days

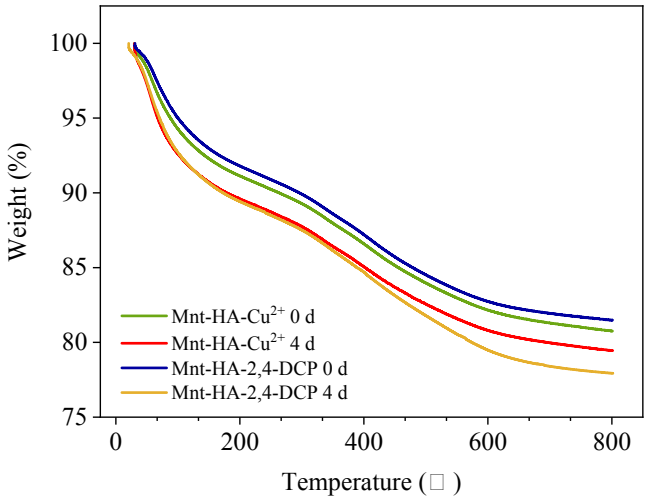

Fig. S5 Thermogravimetric analyses of Mnt-HA-0.1 mM Cu^{2+} and Mnt-HA-2 mM 2,4-DCP samples before and after irradiation for 4 days

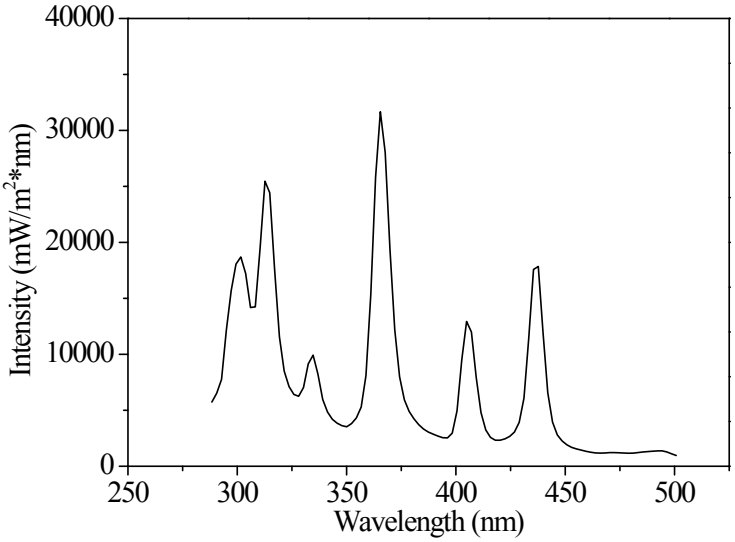

Fig. S6 Spectral information of mercury lamp

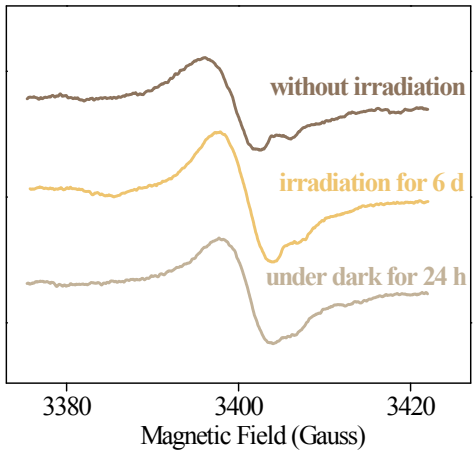

Fig. S7 EPR spectrum of 0.04 Mnt-HA samples without irradiation, irradiation for 6 days and under dark for 24 hours after irradiation.

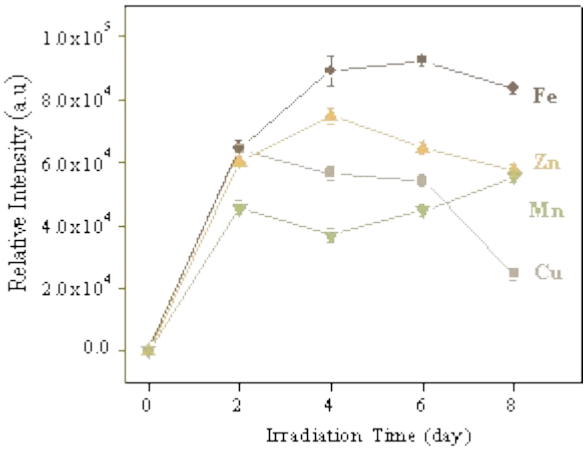

Fig. S8 Relative intensity trend of EPR signal in Mnt-HA complex with different transition metal ions (Cu^{2+}, Fe^{3+}, Zn^{2+}, and Mn^{2+}) under different irradiation time

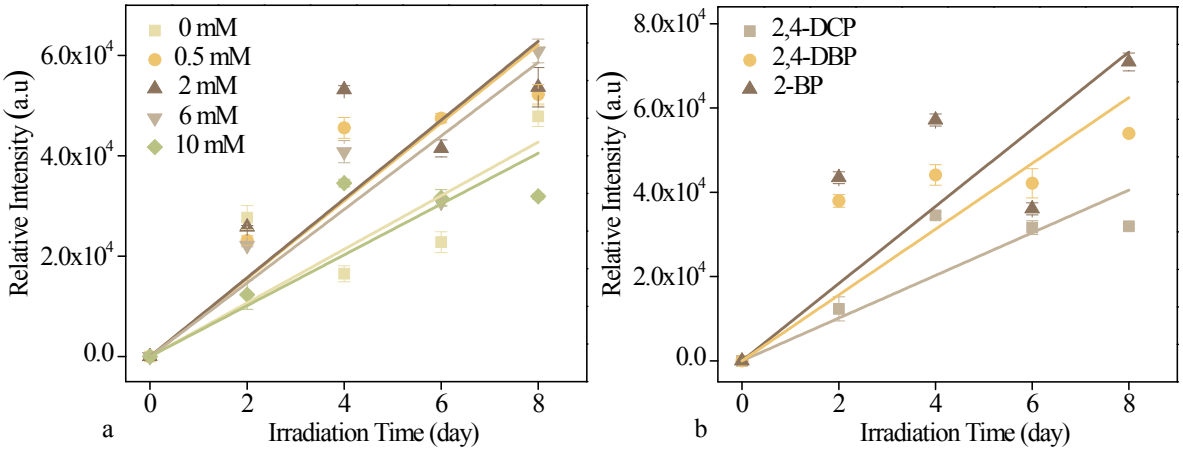

Fig. S9 Influence of halo phenols on the formation of PFRs in Mnt-HA complex: (a) Relative intensity trend of EPR signal in Mnt-HA complex with different concentrations of 2,4-DCP (0, 0.5, 2, 6, 10 mM) under different irradiation time (b) Relative intensity trend of EPR signal in Mnt-HA complex with different halo phenols (2,4-DCP, 2,4-DBP, and 2-BP) under different irradiation time

References

1. Y. G. Zhao, H. Y. Shen, S. D. Pan and M. Q. Hu, Synthesis, characterization and properties of ethylenediamine-functionalized Fe3O4 magnetic polymers for removal of Cr(VI) in wastewater, *J Hazard Mater*, 2010, **182**, 295-302.
2. J. Shen, J. Liu, Y. Xing, H. Zhang, L. Luo and X. Jiang, Application of TG-FTIR analysis to superfine pulverized coal, *Journal of Analytical and Applied Pyrolysis*, 2018, **133**, 154-161.
3. J. Ahmed, M. Mulla, Y. A. Arfat and L. A. T. Thai, Mechanical, thermal, structural and barrier properties of crab shell chitosan/graphene oxide composite films, *Food Hydrocolloids*, 2017, **71**, 141-148.
4. U. G. Nwosu, L. Khachatryan, S. G. Youm, A. Roy, A. L. N. dela Cruz, E. E. Nesterov, B. Dellinger and R. L. Cook, Model system study of environmentally persistent free radicals formation in a semiconducting polymer modified copper clay system at ambient temperature, *Rsc Advances*, 2016, **6**, 43453-43462.
5. T. Li, F. Song, J. Zhang, S. Liu, B. Xing and Y. Bai, Pyrolysis characteristics of soil humic substances using TG-FTIR-MS combined with kinetic models, *Sci Total Environ*, 2020, **698**, 134237.
6. S. Wang, B. Gao, Y. Li, A. Mosa, A. R. Zimmerman, L. Q. Ma, W. G. Harris and K. W. Migliaccio, Manganese oxide-modified biochars: preparation, characterization, and sorption of arsenate and lead, *Bioresour Technol*, 2015, **181**, 13-17.